Synthesis and Characterization of Ground Biochar (GB) Reinforced Composites for Removal of Heavy Metal from Palm Oil Mill Effluent (POME)

Md Rezaur Rahman,[a,*] Anthonette Anak James,[a] Hadi M. Marwani,[b] Sinin bin Hamdan,[a] Khairul Anwar bin Mohamad Said,[a] Muhammad Khusairy Bin Bakri,[a,c] Jamal Uddin,[d] Mohammed Mahbubul Matin,[e] O. Madkhali,[f] Mahmood D. Aljabri,[g] and Mohammed M. Rahman [b,*]

Heavy metal contamination ruins the ecosystem and water quality. The adsorption method for heavy metal remediation is preferred because of its low cost and high efficiency. This work created eco-friendly ground biochar (GB) biomass-based derivatives reinforced polylactic acid (PLA) with titanium dioxide (TiO_2). The composites improved palm oil mill effluent (POME) conditions, and H_2SO_4 activation increased pores by 80%. PLA and TiO_2 altered GB characteristics, according to FTIR analysis. A significant adhesion interaction showed that GB, PLA, and TiO_2 particles were compatible. Ball milling's shear force increased surface area, according to Brunauer-Emmett-Teller (BET) research. Particle size reduction increased GB porosity. Scanning electron microscopy (SEM) was used to study the porous structure of GB and the synergistic effect of PLA and TiO_2 on POME during treatment. The SEM showed several components on the composite surface, demonstrating its efficacy. Atomic absorption spectroscopy (AAS) showed that sample C's composite, which had the most GB, decreased POME heavy metals by 94.4% manganese (Mn), 88.4% cadmium (Cd), and 94.4% zinc (Zn). The resulting POME met the Malaysian Department of Environment's POME discharge limit by reducing chemical oxygen demand (COD), total suspended solids (TSS), turbidity, and pH.

DOI: 10.15376/biores.18.3.5548-5573

Keywords: POME; Heavy Metals; Adsorption; Nano-activated Carbon; Composites

*Contact information: a: Department of Chemical Engineering and Energy Sustainability, Faculty of Engineering, Universiti Malaysia Sarawak (UNIMAS), 94300 Kota Samarahan, Sarawak, Malaysia; b: Department of Chemistry, King Abdulaziz University, Jeddah 21589, Saudi Arabia and Center of Excellence for Advanced Materials Research (CEAMR), King Abdulaziz University, Jeddah 21589, Saudi Arabia; c: Composite Materials and Engineering Center, Washington State University, 2001 East Grimes Way, 99164, Pullman, Washington, U.S.A.; d: Department of Natural Science, Coppin State University, Science and Technology Center, Baltimore, Maryland, 21216, U.S.A.; e: Bioorganic and Medicinal Chemistry Laboratory, Department of Chemistry, Faculty of Science, University of Chittagong, 4331 Chittagong, Bangladesh; f: Department of Physics, College of Science, Jazan University, P.O. Box 114, Jazan 45142, Kingdom of Saudi Arabia; g: Department of Chemistry, University College in Al-Jamoum, Umm Al-Qura University, Makkah 21955, Saudi Arabia; *Corresponding author: rmrezaur@unimas.my*

INTRODUCTION

Based on the current global production volume, Malaysia is the second largest palm oil producer, with one-third of the world's palm oil (Hirschmann 2022; Shahbandeh 2022). The increased demand for palm oil has increased the generation of palm oil mill effluent

(POME). There are several challenges regarding the discharge of POME to water bodies. Such effluents often do not comply with the Environmental Quality Act 1974 (EQA 1974) discharge limit (Zahari *et al*. 2017; Kamyab *et al*. 2018; Mosunmola and Olatunde 2020; Mohammad *et al*. 2021). Although POME is classified as a non-toxic industrial effluent, raw POME contains a high level of chemical oxygen demand (COD), biochemical oxygen demand (BOD), organic and inorganic contaminants, as well as suspended solids, which can pollute the environment and harm the aquatic ecosystem (Lim *et al*. 2020; Mohammad *et al*. 2021). In Malaysia, most POME treatments use the traditional ponding system because it has low capital and operating costs. However, this method raises concerns about the low treatment effectiveness and the required large surface area (Kaman *et al*. 2017).

Biodegradable and sustainable adsorbents have the potential to reclaim a higher quality of treated POME. The carbonaceous adsorbent is an eco-friendly material that has a great pore structure with a large surface area, allowing them to remove high percentages of organic and inorganic contaminants (Ahmad and Azam 2019). Jahromi and Ghahreman (2019) discovered that acid pre-treatment improves adsorption properties by increasing adsorbent porosity and surface area. One of the advantages of carbonaceous adsorbent is that it offers regeneration and reuse for multiple cycles in adsorption processes (Alsawy *et al*. 2022; Baskar *et al*. 2022). The regeneration and reuse approach of adsorbents plays a vital role in improving the cost-effectiveness and sustainable approach that aligns with the Sustainable Development Goals (SDGs). Although the concept of adsorbent regeneration and reusability appears promising, more research and validation are required to assess the economic feasibility of adsorbent regeneration, especially on the operational cost and energy requirements. In addition, there must be a plan for how to deal with concentrated brines collected during the regeneration process. Studies have considered the effect of the regeneration cycle on the adsorbent properties and potential savings compared to using new adsorbents before assessing the overall performance of adsorbent regeneration (Moosavi *et al*. 2020; Alsawy *et al*. 2022; Santos *et al*. 2022).

The search for effective natural-based adsorbent materials has consistently been a vibrant field of study. Several studies have demonstrated the effectiveness of carbonaceous-based composites as adsorbents in removing heavy metals (*e.g*., cadmium (Cd), lead (Pb), chromium (Cr), mercury (Hg), arsenic (As), zinc (Zn), iron (Fe)) from industrial effluent via adsorption (Gul *et al*. 2021; Kumar *et al.* 2021; Mahesh *et al.* 2022). However, the existing studies still show a lack of information regarding the adsorption of various heavy metals from POME using composites derived from polylactic acid (PLA) and titanium dioxide (TiO_2) with ground biochar-adsorbent to overcome the limitation of conventional adsorbents where the interaction between the process parameters has been restricted. This research aims to create ground biochar (GB) carbonaceous adsorbent from pine sawdust via a pyrolysis process and sulphuric acid (H_2SO_4) activation. The ball milling process is performed to reduce the particle size of the adsorbent for better porosity development and a larger surface area. The synergic effects of GB-adsorbent-reinforced PLA with TiO_2 photocatalytic behaviour were examined by looking at the efficacy of the adsorption process. PLA was chosen due to its biodegradable derived properties, while TiO_2 can help minimize the brittleness, fading, and cracking that can occur in plastics and other materials as a result of light exposure. TiO_2 also has high heavy uptake, chemical stability, wide bandgap, high refractive index, nontoxic, and high catalytic activity. The analyses included Fourier transform infrared spectroscopy (FTIR), scanning electron microscopy (SEM) with energy dispersive X-ray spectroscopy (EDX), and the Brunauer-Emmett-Teller (BET) method. Together, these methods made it possible to observe the

functional groups, morphology, elemental composition, and porosity of the composite. Furthermore, the study also employed atomic absorption spectroscopy (AAS) to observe the performance of the composites in eliminating the pollutants from raw POME. In addition, in-depth analysis and comparison are also performed to validate the performance of the prepared composites against other results.

EXPERIMENTAL

Materials

The poly(lactic) acid (CAS Number: 26100-51-6), titanium (IV) oxide (CAS Number: 13463-67-7), sulphuric acid (CAS Number 13813-19-9), and sodium bicarbonate ($NaHCO_3$) (CAS Number 144-55-8) were supplied by Sigma-Aldrich Sdn (Petaling Jaya, Malaysia). The pine sawdust was provided by Vyatka State University, Kirov, Russia. The POME was obtained from FELCRA, Kota Samarahan, Sarawak.

Methods

Figure 1 displays a flowchart outlining the various steps taken during the experiment. The subsequent elaboration of each step is described on the following page.

Pine sawdust adsorbent preparation

The pine sawdust was imported from Russia by Vyatka State University, Kirov, Russia. It was washed thoroughly with deionized water to remove excess dirt and impurities. Next, the samples were kept in an oven at 50 °C overnight. Later it was stored in an airtight container. The sample was ground and sieved to reduce the particle size between 0.38 to 0.3 mm to improve the activation reaction (Senturk and Yildiz 2020).

Pre-treatment of pine sawdust

First, 20 g of sample was pre-treated and activated with 200 mL of H_2SO_4 acid solution in a 500 mL conical flask. The mixture was then heated in a muffle oven at 150 °C for a period of 24 h. Once the carbonization was completed, the sample was washed with deionized water and soaked overnight in a 1% $NaHCO_3$ solution to reduce the sample acidity (Senturk and Yildiz 2020). The sample was filtered using vacuum filtration to obtain the residue and then washed using deionized water several times until it reached pH 7. The residue was distributed evenly on a plate to ensure equal heat distribution from the oven. The operating conditions were the same as before.

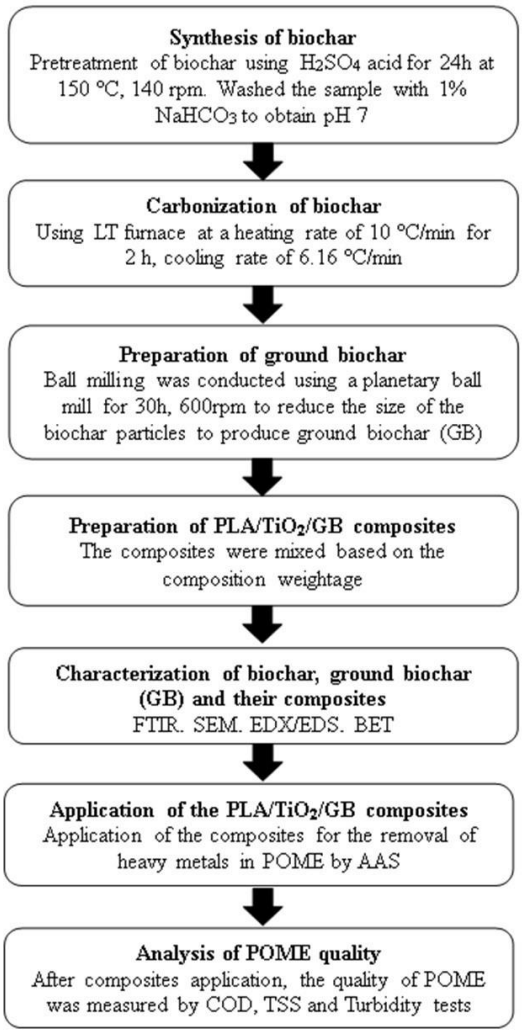

Fig. 1. Overview of the experimental steps

Carbonization of pine sawdust

Upon carbonization, the sample was first placed into a ceramic bowl wrapped with aluminium foil and then covered with a layer of clay before putting it in LT Furnace (Selangor, Malaysia). The temperature was ramped from room temperature to 200 °C, then increased to 400 °C at a heating rate of 10 °C/min for 2 h, during which the carbonization process occurred. After the carbonization process, LT Furnace was cooled at a cooling rate of 6.16 °C/min until it reached room temperature. The sample was collected the next day and further sieved using a 300 µm sieve. The sample was labelled as biochar sample.

Preparation of ground biochar (GB) via ball milling process

Approximately 10 g of biochar were ground for 10 min at a speed of 250 rpm using a grinder. The biochar was poured into a half-capacity cylindrical steel ball mill jar. Ten stainless-steel balls weighing 0.5 g each were used to reduce the particle size of biochar in the Planetary Ball Mill (PM 400) jar. The process took about 30 h at a speed of 600 rpm, and the sample was removed for testing at regular intervals to ensure it reached the nanoscale. The sample was labelled as ground biochar (GB) sample.

PLA/TiO_2/GB composites preparation

The PLA, TiO_2, and GB were mixed based on the composition weightage tabulated in Table 1.

Table 1. Composites Weightage Factors

Sample	Component 1 PLA (g)	Component 2 TiO_2 (g)	Component 3 GB (g)
A	97	2	1
B	96	2	2
C	95	2	3

Application of PLA/TiO_2/GB composites with POME via solution mixing

The POME was collected from Felcra Samarahan Jaya Palm Oil Mill, Kota Samarahan, Sarawak, and the initial conditions of POME, such as pH, COD, turbidity, and TSS, were evaluated. In each conical flask, 100 mL of POME was poured and added to the sample. Each conical flask was labelled as samples A, B, and C. The samples were placed in the auto-shaker for 48 h of contact time at 180 rpm at room temperature. After the end of the contact time of 48 h, the samples were removed from the auto-shaker and were filtered using 0.55 µm filter paper with a vacuum pump to obtain the residues for further analysis.

Characterizations

Fourier transform infrared (FTIR) spectroscopy

The functional groups of the samples were examined using an IRAffinity-1 FTIR spectrophotometer (Shimadzu, Kyoto, Japan) via the observation of IR spectrum bands with 32 scannings ranging from 400 to 4000 cm^{-1}. First, a sample pellet for FTIR spectroscopy was made using a 1:5 ratio of the specimen to potassium bromide (KBr) powder on a small pestle. The pelletized sample was extracted and placed inside the FTIR spectroscopy sample holder. The FTIR analysis was carried out following ASTM E1252-98 (2021) and ASTM E168-16 (2016) standards.

Scanning electron microscopy (SEM)

The morphological images of the samples, especially the pore structure, were evaluated *via* a Hitachi analytical tabletop SEM (benchtop) (TM-3030, Hitachi High Technologies, Mannheim, Germany). The specimens were mounted on aluminium stubs and were fine-coated using auto fine coater JFC-1600 (Jeol, Tokyo, Japan). The morphological images of the sample were captured using a field emission gun with an acceleration voltage of 5 and 15kV. The procedure for the SEM analysis was conducted following the ASTM E2015-04 (2014) standards.

Energy X-Ray Dispersive Spectroscopy (EDX/EDS)

EDX analysis (Quantax75TM Series Energy Dispersive X-Ray Spectrometer by Hitachi Ltd., Tokyo, Japan) was used to determine the elementary material composition present on the surface of the samples, which was correlated with SEM images produced for the respective sample.

Brunauer-Emmett-Teller (BET)

The BET analyzer was used to measure the specific surface area of each sample based on the ASTM D6556-14 (2014) standard. The degassing condition of the sample was 1 to 3 h at 300 °C. Several repeated tests were carried out to obtain the most representative outcomes. The micropore volume was calculated using the Dubinin-Radushkevich (DR) equation, while the pore volume was calculated using the plotted graph of N_2 adsorption isotherms of biochar and ground biochar. The equations are as follows (Tran *et al*. 2017). Total pore volume (V_{Total}) is given by Eq. 1,

$$V_{\text{Total}} = \frac{Q_{0.99}}{647} \quad (1)$$

Average pore diameter (L_0), is given by Eq. 2,

$$L_0 = \frac{4\ X\ V_{Total}}{S_{BET}}\ X\ 1000 \quad (2)$$

The Dubinin-Radushkevich (DR) equation for characteristic adsorption energy (E_0) is presented as Eq. 3,

$$E_0 = \frac{10.8}{L_0}\ X\ 11.4 \quad (3)$$

Gaussian distribution ($\frac{V_{Micro}}{V_{Total\ micro}}$) for micropore volume estimation is given by Eq. 4,

$$\frac{V_{Micro}}{V_{Total\ micro}} = \exp\left\{-\left(\frac{E}{E0}\right)^2\right\} \quad (4)$$

where $E = RT \ln\left(\frac{p}{p^0}\right)$ (5)

In the foregoing equations, V_{Total} is the total pore volume (cm^3g^{-1}); $Q_{0.99}$ is the quality absorbed volume (cm^3g^{-1}STP) at 0.99 of the relative pressure ($\frac{p}{p^0}$); S_{BET} is the BET specific surface area (m^2g^{-1}); L_0 is the average pore diameter (nm); E_0 is the characteristic adsorption energy ($kJmol^{-1}$); V_{Micro} is the Micropore volume (cm^3g^{-1}); $V_{Total\ micro}$ is the total micropore volume (cm^3g^{-1}); and E is based on the Polanyi equation (Buttersack *et al.* 2016).

Atomic absorption (AAS) spectroscopy

The heavy metal concentrations (Mn, Cd, Zn, Fe) in raw and final POME were investigated using a flame AAS 'AA-7000' spectrometer (Shimadzu, Japan). The calibration solution was obtained from Sigma-Aldrich Sdn (Petaling Jaya, Malaysia). The observations were made according to the electromagnetic radiation wavelength emitted by the light source produced by the equipment. The test was done according to the ASTM D7740-20 (2020) standard.

Chemical oxygen demand (COD)

A total of 2.0 mL of POME solution and distilled water were added to two different vials. The distilled water was spared as a "blank sample". The caps of the vials were closed tightly, and both were shaken gently to mix the samples. The vials were placed in a COD digester (DRB200 Reactor) for heating. The temperature was set at 150 °C for 2 h. The vials were removed after 2 h from the COD digester and were cooled at room temperature.

The COD values were measured using HACH DR900 and recorded. It is noted that potassium dichromate ($K_2Cr_2O_7$) in combination with boiling sulfuric acid (H_2SO_4) has been commonly used as an oxidant in COD assays. This test was done according to ASTM D1252-06 (2020).

Total Suspended Solid (TSS) and Turbidity Test

First, 10 mL of deionized water was poured into a sample cell and served as a blank sample to calibrate the TSS and turbidity reading to 0.00 mg/L and 0.00 FAU. After calibration, 10 mL of raw POME was poured into a sample cell. Before inserting the sample cell into the cell holder, it was thoroughly cleaned. The "read" button was pressed to measure the TSS and turbidity value of the sample. This procedure was repeated for all treated POME samples. This test was done according to ASTM D5907-18 (2018).

RESULTS AND DISCUSSION

Infrared Spectral Properties

The FTIR analysis presented in Fig. 2 shows the presence of functional groups in both biochar and ground biochar (GB), representing their complex characteristics. A strong and sharp peak was observed at 3741.9 cm^{-1}, indicating strong O-H stretching bands in both biochar and ground biochar samples (Nyuk Khui *et al*. 2020, 2021). According to Senturk and Yildiz (2020), this finding was indeed due to the presence of O-H groups in lignocellulosic materials. It corresponded to water molecules containing O-H hydroxyl groups in corn stalk biomass, characterizing peaks between 4000 cm^{-1} and 3584 cm^{-1} (Salema *et al*. 2017). The medium peaks appearing at 2956.9 cm^{-1} (biochar), 2951.1 cm^{-1} (GB), 2544.1 cm^{-1} (biochar), and 2549.9 cm^{-1} (GB) showed the presence of CH stretching vibration in the methyl and methylene groups. This finding was supported by the rising of symmetric and asymmetric peaks at 2850 cm^{-1} and 2918 cm^{-1} in the FTIR analysis of *Leucaena leucocephala* bark, which refers to the methoxyl groups of lignin (Salim *et al*. 2021).

Senturk and Yildiz (2020) and Wijaya and Wilharto (2020) stated that the alkane functional groups of cellulose, hemicellulose, and lignin introduced C-H bending vibrational modes giving rise to absorbances between 2500 and 3000 cm^{-1}. The peak of 1591.3 cm^{-1} observed in both samples indicated the presence of lignin in pine sawdust, in line with the observations of Wijaya and Wilharto (2020) in cocoa shell pyrolysis and Abel *et al.* (2021) in biochar samples.

The peaks at 1255.7 cm^{-1} (GB) and 1207.4 cm^{-1} (biochar) represented the depolymerization and dehydration of hemicellulose and cellulose in the respective samples. The C≡C stretching vibration that specified the alkyne was identified at peaks of 2166.1 and 2164.1 cm^{-1} of biochar and GB. The peaks between 1400 cm^{-1} and 1750 cm^{-1} presented the features of C=C and C=O of an aromatic ring, which also appeared at 1442 cm^{-1} (Feng *et al*. 2014) and 1587 cm^{-1} (Alfattani *et al*. 2022). Carboxylic acids, esters, and alcohol have been introduced by absorption bands at 1255.7 and 1207.4 cm^{-1}, distinguishing the C-O functional groups. Senturk and Yildiz (2020) explained that these groups were generally found in the molecular structures of the biochar that had been activated by H_2SO_4. Previous researchers mentioned that the formation of peaks between 1250 and 1020 cm^{-1} can also be attributed to the C-N stretching vibration indicating the presence of amines in the samples (Bilal *et al*. 2013; Salim *et al*. 2021).

According to Salim *et al.* (2021) and Ali and Latip (2020), the cyclic nature of the ether by forming an aliphatic C-O stretching band at 1030 cm^{-1} has been identified for both samples at an intensity of 1033.8 cm^{-1}. The absorbance band appears between 675 cm^{-1} and 1000 cm^{-1}, corresponding to the C-H stretching vibration of alkenes, while the bands between 550 cm^{-1} and 730 cm^{-1} represent the C-Cl bending stretching. The results in Fig. 2 indicated that the study of biochar and GB did not reveal any significant changes, as the spectra patterns appeared the same regardless of their transmittance intensities. This result was predicted by Nyuk Khui *et al.* (2020) due to the formation of new pores and increased surface area after the ball milling process. However, the ball milling does not affect the presence of functional groups in the sample, which shows similar effects to the chemical pre-treatment analysis.

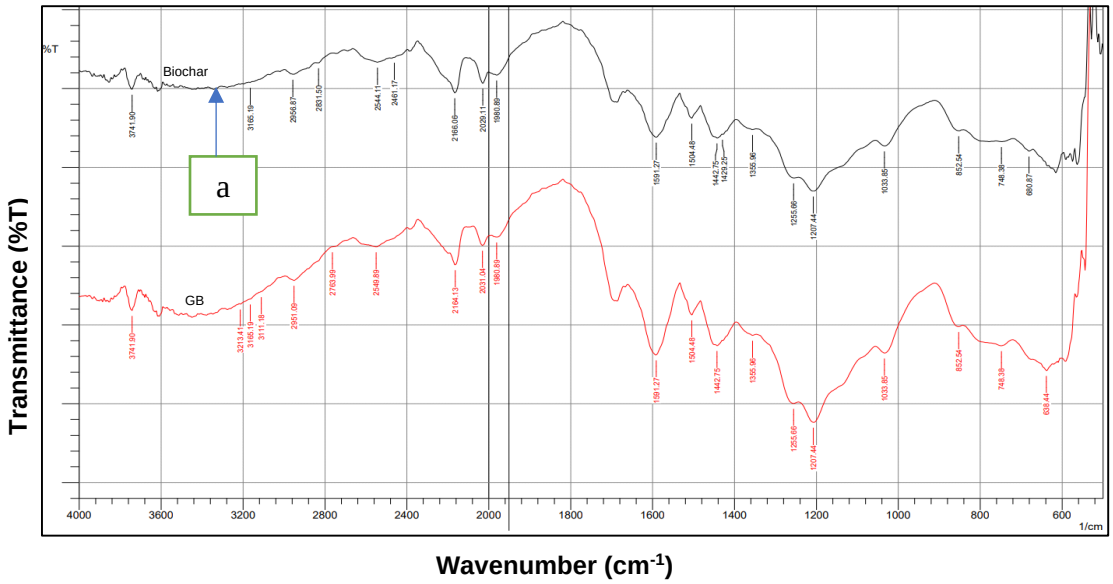

Fig. 2. IR spectra of biochar (black-line) and GB (red-line)

Figure 3 depicts the FTIR spectra of titanium dioxide (TiO_2) and polylactic acid (PLA), while Fig. 4 illustrates the FTIR spectra of three different GB/ TiO_2 /PLA composites labelled as samples A, B, and C. The addition of TiO_2 and PLA to GB was found to influence band intensity characteristics. The functional groups present in the region of 695 to 760 cm^{-1} of Fig. 4 were the features of C=O in PLA. PLA contains C=O groups because it was derived from lactic acid, which has a high carbon chain (Shaharuddin *et al*. 2019). However, the findings of Naayi *et al.* (2018) contradicted that interpretation, defining the adsorption peak between 430 cm^{-1} and 781 cm^{-1} as the Al-O stretching vibration band in alumina. It was detected in all samples at weak absorbance bands of 678.9, 761.9, and 763.8 cm^{-1}, as shown in Fig. 4.

The absorbance bands between 869.9 and 889.2 cm^{-1} were attributed to the ring formation and deformation of C-H out-of-plane of lignin. A wide and broader peak of symmetric and asymmetric -CH_3 vibrations was revealed at peaks 2902.9, 2883.6, and 2933.7 cm^{-1} in all samples. These peaks at 2995 and 2947 cm^{-1} represent the alkyl stretching vibrations of C-H in the PLA polymer chain. A strong O-H stretching vibration was found at peaks of 3211.5 to 3493.1 cm^{-1} in sample A, including 3498.9 to 3414 cm^{-1} in sample B, indicating the presence of alcohol compound in the mixtures. In addition, the peaks at 3425.6 and 3498.9 cm^{-1} also seem to be visible in sample C. Datta *et al.* (2016)

stated that the peaks were caused by the increasing TiO_2 content in the prepared composites, as evidenced by the additional band at 3370 cm^{-1} in their research. Another observed band at 1377.17 cm^{-1} implies that the carboxylate compound occurred with medium vibration of stretching -C-O, as described by Sayuti *et al.* (2021). The medium vibrations at 3226.91 cm^{-1} in sample A and 3234.62 cm^{-1} in sample C were attributed to the stretching bond of N-H, which arise in the same region of alcohol O-H, similar to the previous findings by Kowalczuk and Pitucha (2019). A weak vibration found at peak intensities of 1728.25 cm^{-1} and 1971.25 cm^{-1} shows the aromatic compound properties of PLA. The existence of 1635.64 cm^{-1} in sample C indicates a strong C=O vibration of aldehyde groups where a strong adhesion interaction between the activated carbon and PLA and TiO_2 particles has been observed. Table 2 provides the IR spectra summary of the relevant information obtained from the analysis of the samples.

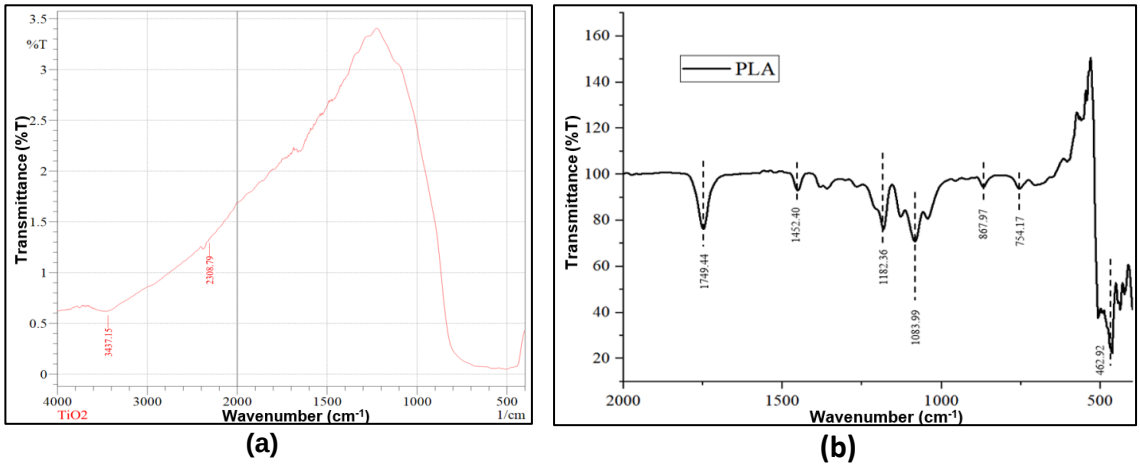

Fig. 3. IR spectra of (a) TiO_2 and (b) PLA

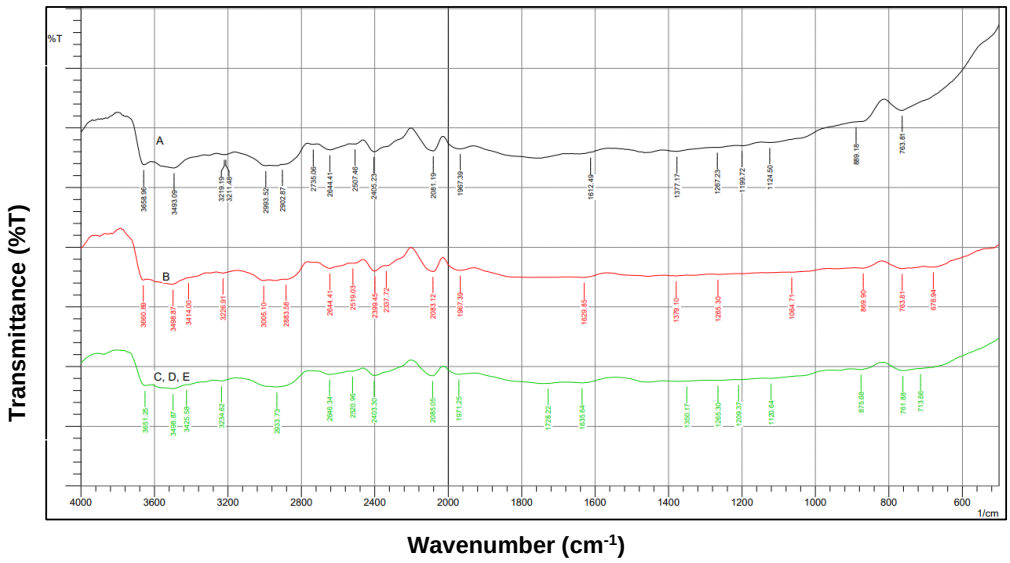

Fig. 4. IR spectra of samples A, B, and C composites.

Table 2. IR Spectra Table by Frequency Range

Wavelength (cm^{-1})	Functional group	Characteristics	Compounds
4000 - 3200	O-H	Stretching	Acid, methanol
3000 - 2500	C-H	Stretching	Alkane
2900-2800	C-H	Stretching	Aldehyde
2260 – 2160	C≡C	Stretching	Alkyne
2000-1650	C-H	Bending	Aromatic compound
1750-1735	C=O	Stretching	Aromatic ring
1760 - 1630	C=O	Stretching	Aldehyde group
1640 – 1535	C=C	Stretching	Conjugated alkene
1400	C=C	Stretching	Aromatic ring
1390-1310	O-H	Bending	Carboxylic acid
1310 - 1250	C-O	Stretching	Aromatic ester
1250 - 1020	C-N	Stretching	Amine
1000 - 675	C-H	Bending	Alkene
900-700	C-H	Bending	Aromatic hydrogen
760-695	C=O	Stretching	Carbonyl group
730-550	C-Cl	Bending	Halo compound

Morphological and Porosity Properties

SEM was used to examine the samples to determine the surface morphologies of both biochar and ground biochar (GB). The SEM image of biochar shown in Fig. 5(a) at 400x magnification displayed multiple microfibrils with irregular sizes, showing open pores with diameters ranging from 15 to 20 µm, whereas Fig. 5(b) shows numerous appearances of small particulates, but they are too small to be seen clearly in the micrograph due to the micro-nano scales pores after ball milling. The outcome of the SEM analysis shown in Fig. 5(b) shows more pronounced particles' deformation at 30 h of milling times, changing the sample morphology due to the shear force applied by the metallic balls on the surface of biochar particles in the mono planetary stainless-steel jar. This result followed other researchers who showed significant particle size reduction after periods of ball milling (Phanthong *et al.* 2018; Lyu *et al.* 2018; Qanytah *et al.* 2020). However, the particle size remained constant after 30 h of milling, as no further changes were observed. The result was similar to findings by Shan *et al*. (2016), who reported that coconut shell-based activated carbon particle size remained the same even after increasing the milling time. Qanytah *et al*. (2020) added that a longer milling process reduces the sample crystallinity, producing an amorphous sample, as displayed in Fig. 5. This may initiate agglomeration of biochar to form large particulates. Despite the disadvantage of a longer milling time, this approach can increase the adsorption capabilities of biochar by creating numerous pores on its surface (Hu *et al*. 2019), leading to an increase in reactivity as the volume ratio of the sample increases (Qanytah *et al*. 2020). Besides, it also increases the contact surface area and leaves numerous vacant pores (Qanytah *et al*. 2020; Abbas *et al*. 2021). The BET analysis in Table 3 reflected this assertion.

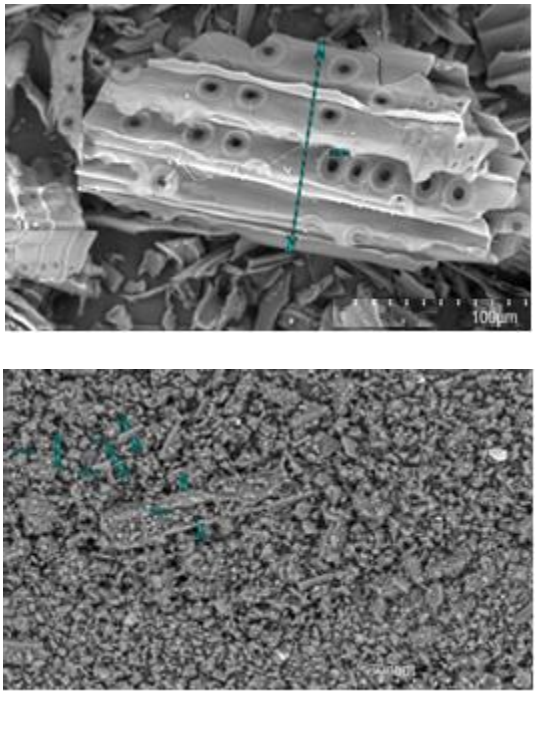

Fig. 5. SEM images at x400 magnification for a) biochar and b) GB

Table 3 shows the specific surface area, total pore volume, micropore volume, and average pore diameter of samples that were obtained from the N_2 adsorption isotherms graph in Fig. 6. According to the results, GB was fivefold higher in surface area than biochar, rising from 5.09 m^2g^{-1} to 25.8 m^2g^{-1}. This result demonstrated the efficiency of ball milling in reducing particle size from the micro to the micro-nano scale (Nyuk Khui *et al*. 2020). Based on the comparison, GB particles have a higher specific surface area than biochar particles, indicating a better porosity of the composite material. The specific surface area of the sample was calculated using the amount of adsorbate gas corresponding to a monomolecular layer on the surface. The results showed that the GB sample had a significant micropore volume, accounting for approximately 90% of the total pore volume. This finding implies that the GB sample contained numerous micropores and some mesopores, which is similar to the findings of Hidayu *et al.* (2013).

Table 3. Specific Surface Area (S_{BET}), Total Pore Volume, Micropore Volume, and Average Pore Diameter of Samples

Sample	S_{BET} (m^2g^{-1})	Total Pore vol ($cm^3\ g^{-1}$)	Micropore Vol ($cm^3\ g^{-1}$)	Average Pore Diameter (Å)
Pine sawdust-biochar	5.093	0.0355	0.001	27.8814
Pine sawdust-ground biochar (GB)	25.779	0.0695	0.0625	10.7839

The nitrogen adsorption/desorption isotherms at 77 K on both biochar and GB at a degassing temperature of 300 °C are shown in Fig. 6. The trend line of the isotherm curves generated by the BET was determined by the pore characteristic and size presented on the surface of the adsorbent (Phothong *et al*. 2021). Although the adsorbents seem porous, the BET analysis result of biochar exhibited Type V isotherms, specifying a not common and weak interaction between absorbate-absorbate. In comparison, the GB trend line showed a gradually increasing trend to the end of relative pressure, displaying the characteristics of both Types I and V isotherms of microporous and mesoporous materials. In addition, the findings illustrated the hysteresis loop of Type H4 at relative pressures greater than 5, showing the formation of slit-like pores on the surface of GB. This discovery implies that the GB sample has been linked to capillary condensation in well-formed mesoporous structures (Allwar 2012).

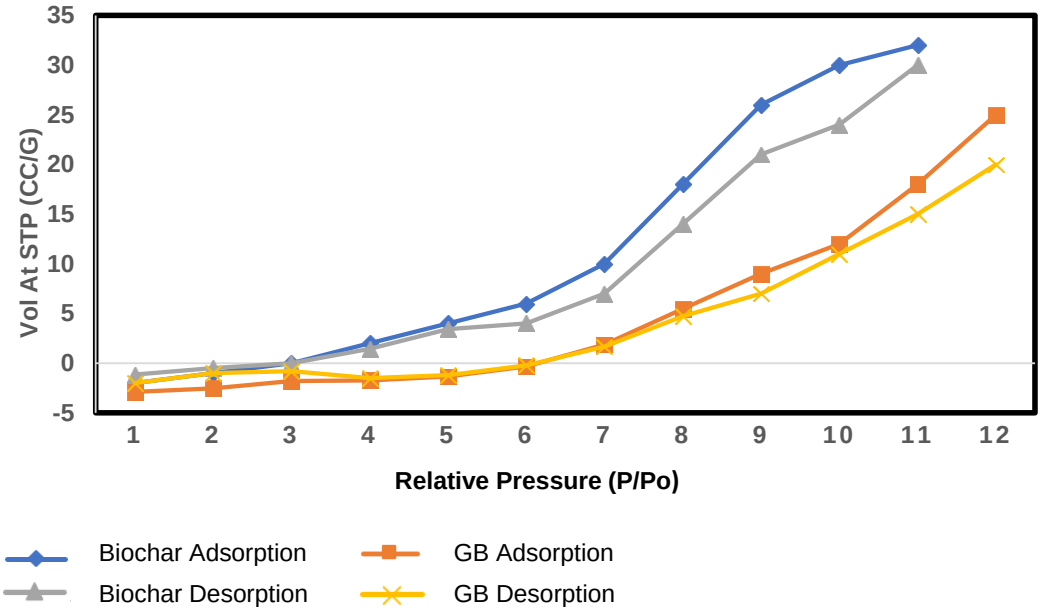

Fig. 6. N_2 adsorption isotherms of biochar and ground biochar (GB)

The morphological images in Fig. 7 present the distribution of PLA/TiO_2/GB composites on the surface of each sample. As per observations, all samples had scattered and irregular shape particles with small white flakes referring to TiO_2 nanoparticles. The TiO_2 nanoparticles and GB particles on the PLA matrix clumped together and blocked the pores of the mixture composites because of poor dispersion issues. The high surface energy and excessive TiO_2 loading also prompted agglomeration problems (Zain *et al*. 2021; Xing *et al*. 2016). It is said that TiO_2 nanoparticles were easier to trap in the pores of activated carbon due to their small size (Matteis *et al*. 2020). Saffar *et al*. (2014) added to the previous statement that aggregation was also initiated by the O-H hydrophilic groups adhering to each particle via the network of hydrogen bonds.

Additionally, the hydrophobic property of PLA affected the compatibility of mixtures due to the weak interaction. Similar circumstances were encountered by Raquez *et al*. (2013), where poor mixture dispersion was noticed when adding TiO_2 nanoparticles with PLA. However, according to Kaseem *et al*. (2019), chemically functionalizing TiO_2 nanoparticles or treating surfaces with alkyl amine and propionic acid can enhance homogeneous dispersion.

The morphological images of the composites shown in Fig. 8 have been evaluated after a 48-h continuous POME adsorption procedure. All sample surfaces shown in Fig. 8 contain impurities, which means that the sample micropores and macropores have been adsorbate-filled.

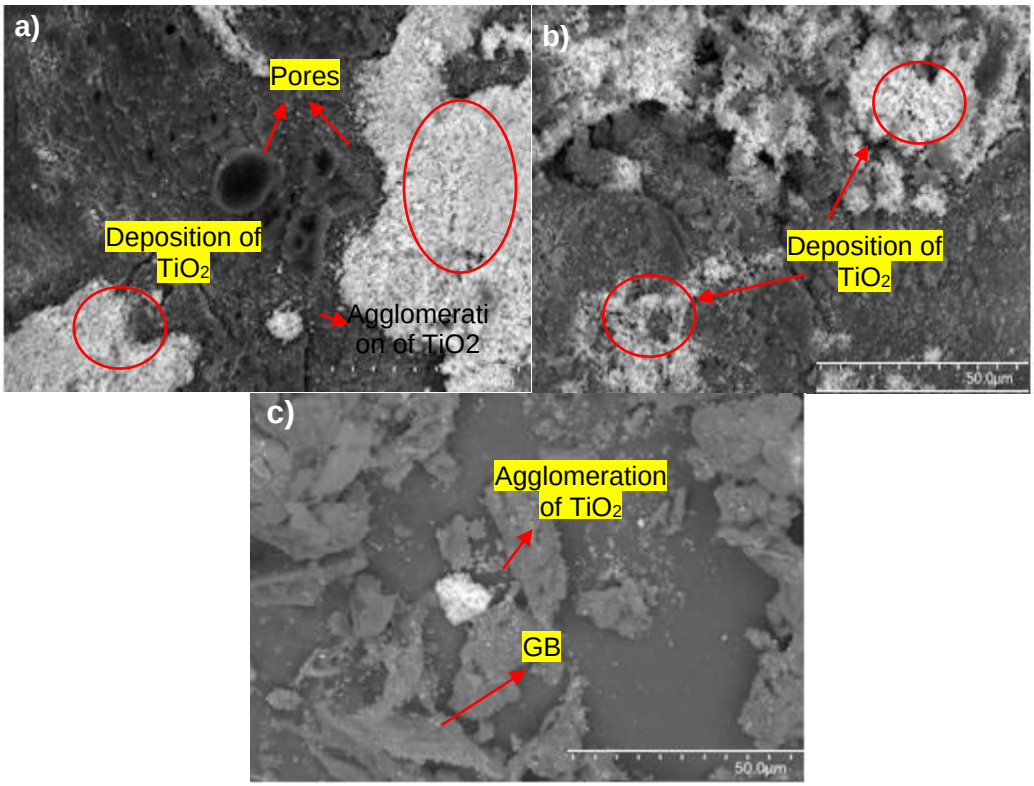

Fig. 7. SEM images at x1000 magnification for samples A, B, and C before POME treatment

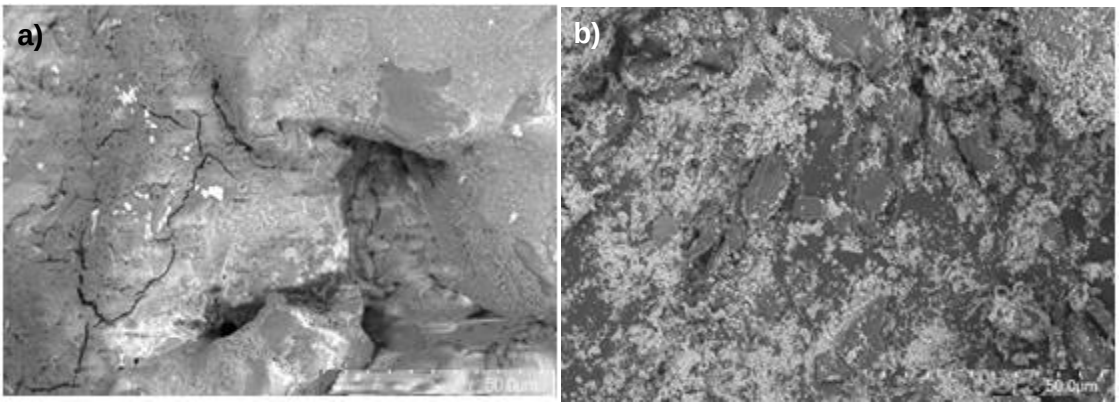

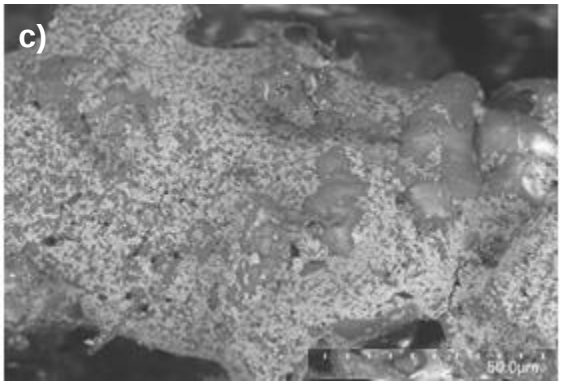

Fig. 8. SEM images at x1000 magnification for samples A, B, and C after POME treatment

Elemental Composition Properties

EDS/EDX analysis

The EDX spectrum results displayed in Figs. 9, 10, and 11 show the presence of elements on the surface of the composites. The comparison of the elemental compositions for each sample based on the EDX peaks has been summarized in Tables 4, 5, and 6**.**

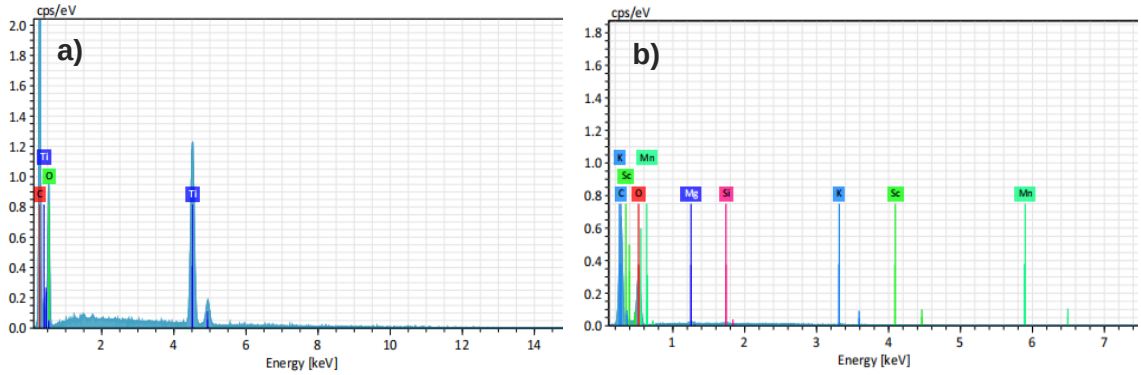

Fig. 9. EDX diffraction spectra of sample A (a) raw unused sample, (b) treated POME

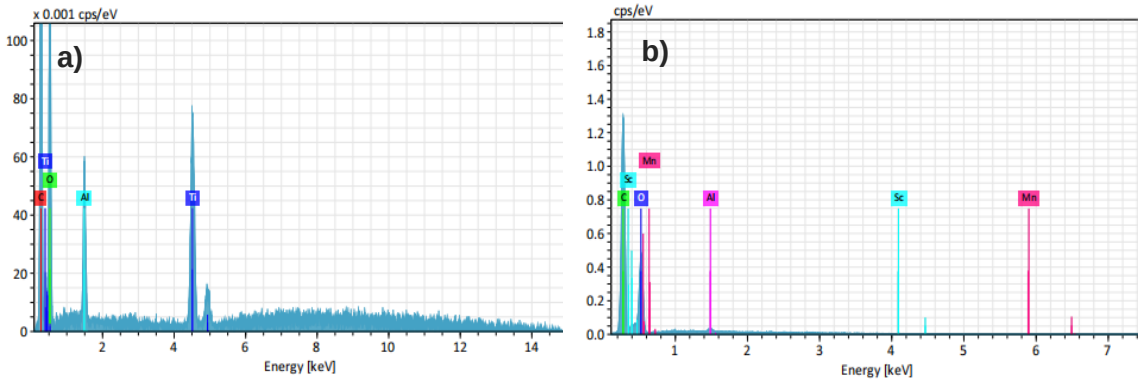

Fig. 10. EDX diffraction spectra of sample B (a) raw unused sample, (b) treated POME.

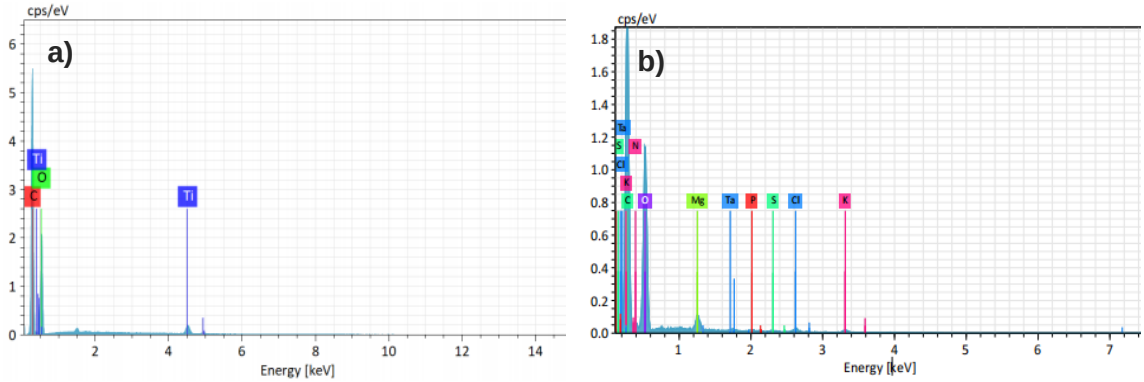

Fig. 11. EDX diffraction spectra of sample C (a) raw unused sample, (b) treated POME.

Three main elements were identified in all samples, namely carbon (C), oxygen (O), and titanium dioxide (TiO_2). Similar to the findings of other researchers, carbon (C) had the highest appearance percentage on the surface composite, followed by oxygen (O). Alam *et al*. (2021) recorded 83% of C and 13% of O in the EDX analysis of activated carbon derived from Paulownia Tomentosa wood, indicating that C and O were the predominant elements in the respective sample. The results in Table 5 also revealed the presence of Al, which may have represented the impurities in raw sample B that resulted from ambient contaminants during sample preparation. The Al may have represented the impurities in raw sample B that resulted from ambient contaminants during sample preparation. This finding is reflected in the FTIR analysis of GB/TiO_2/PLA, where the appearance of Al-O stretching vibration has been observed. The AAS analysis provides additional insight into the synergistic impact of adsorption and photocatalytic degradation of the organic pollutants. By looking at the comparison of EDX outcomes tabulated in Tables 4, 5, and 6, it has been possible to identify the contaminants adhering to the samples' pores shown in Fig. 8 of the SEM result after POME treatment. The C and O made up the highest element but at lower rates after POME treatment. As more pollutants were deposited, the percentages of C and O fell from their initial values, as recorded by all samples. The EDX results were comparable to those from Zain *et al*. (2021), demonstrating the decrease in C content due to particulate deposition on the surface of the composite. It signifies sample C's superiority over samples A and B in removing pollutants from raw POME.

Table 4. EDX Comparison Analysis for Sample A

Sample	Elemental Mass (%)							
	C	O	Ti	Sc	Mn	K	Si	Mg
A (raw)	62.4982	43.2898	2.2974	-	-	-	-	-
A (treated)	60.6372	38.2131	-	0.0075	0.0075	3.19	2.0363	1.6765

Table 5. EDX Comparison Analysis for Sample B

Sample	Elemental Mass (%)					
	C	O	Ti	Al	Sc	Mn
B (raw)	54.4128	60.0801	21.5051	4.7274	-	-
B (treated)	50.1992	42.8830	-	1.1470	0.0014	0.0014

Table 6. EDX Comparison Analysis for Sample C

Sample	Elemental Mass (%)									
	C	O	Ti	K	N	Mg	Cl	Ta	P	S
C (raw)	45.310	37.202	4.484	-	-	-	-	-	-	-
C (treated)	33.993	29.820	-	4.695	2.468	1.936	1.84	0.562	0.418	0.351

AAS analysis

An AAS study was used to investigate the effectiveness of the developed PLA/TiO_2 /GB composites by assessing the uptake of heavy metals in POME to meet the regulatory discharge limit stated in the Environmental Quality Regulations 1977 (Prescribed Premises for Crude Palm Oil), as shown in Fig. 12. Several heavy metals, such as Mn, Cd, Zn, and Fe, were investigated to observe the developed composites' efficiency in removing the highest percentage of heavy metals. The initial and final concentrations of heavy metals in the respective POME are shown tabulated in Table 7. The findings revealed that sample C achieved the highest removal percentage of Mn, Cd, and Zn with efficiencies of 94.4%, 88.4%, and 94.4%, respectively. In comparison, sample B showed the most significant reduction of Fe with 56.4%. Based on the comparative studies, the reduction percentage of Mn by sample C was 1.9% higher than using alum, as shown by Jagaba *et al*. (2020). This achievement refutes the assertion that bio-sorbents necessarily have a low adsorption capacity (Jagaba *et al*. 2020). However, Pertile *et al*. (2021) stated that the low ability of bio-sorbent adsorption only applies to untreated biosorbents, not chemically modified biosorbents.

Furthermore, the heavy metal adsorption rate distinction was also influenced by the industrial effluent used and its concentration. Not much difference was found for the reduction of Zn from POME either by using sample C or activated carbon derived from coconut shells and cow bone powder (Adeleke *et al.* 2017). Adding a high dosage of ground biochar pine sawdust during sample preparation provides more potential for treating POME as a higher tendency of heavy metal ions adhered to the free pore sites, allowing a greater adsorption rate. However, a few researchers have argued that further increasing the weight percentage of adsorbent will not further influence the removal percentage of heavy metals as it has already reached saturation (Pertile *et al.* 2021; Sreedhar and Reddy 2019; Gupta *et al*. 2021). Adeleke *et al.* (2017) demonstrated this claim by observing a decreasing pattern of heavy metal uptake as activated carbon content increases. Sreedhar and Reddy (2019) also noticed a similar decreasing trend of adsorption capacity when the adsorbent dosage was increased. The effect is probably due to the concentration gradient and increased blockage of available active sites caused by the agglomeration of GB particles that reduces the specific surface area of the sample. Furthermore, the repulsion between free metal ions in POME and adsorbed ions reduced additional heavy metal adsorption (Taha *et al*. 2016). Other factors that affect the elimination of contaminants from POME

are such as contact time (Aziz *et al*. 2021), agitation speed (AlMoharbi *et al*. 2019), and initial pH (Abbar *et al*. 2017; Khamis and Jalil 2021).

Table 7. The Initial Concentration of POME

Heavy Metal	Initial Concentration (ppm)	Final Concentration (ppm)			Percentage Absorption (%)		
		Sample A	Sample B	Sample C	Sample A	Sample B	Sample C
Manganese (Mn)	2.7059	0.7680	0.4189	0.3146	34.72	76.39	94.44
Cadmium (Cd)	0.0720	0.0047	0.0017	0.0004	71.62	84.52	88.37
Zinc (Zn)	1.4915	0.1346	0.1018	0.0832	90.98	93.17	94.42
Iron (Fe)	1.8230	0.8192	0.7949	0.8271	55.06	56.39	54.62

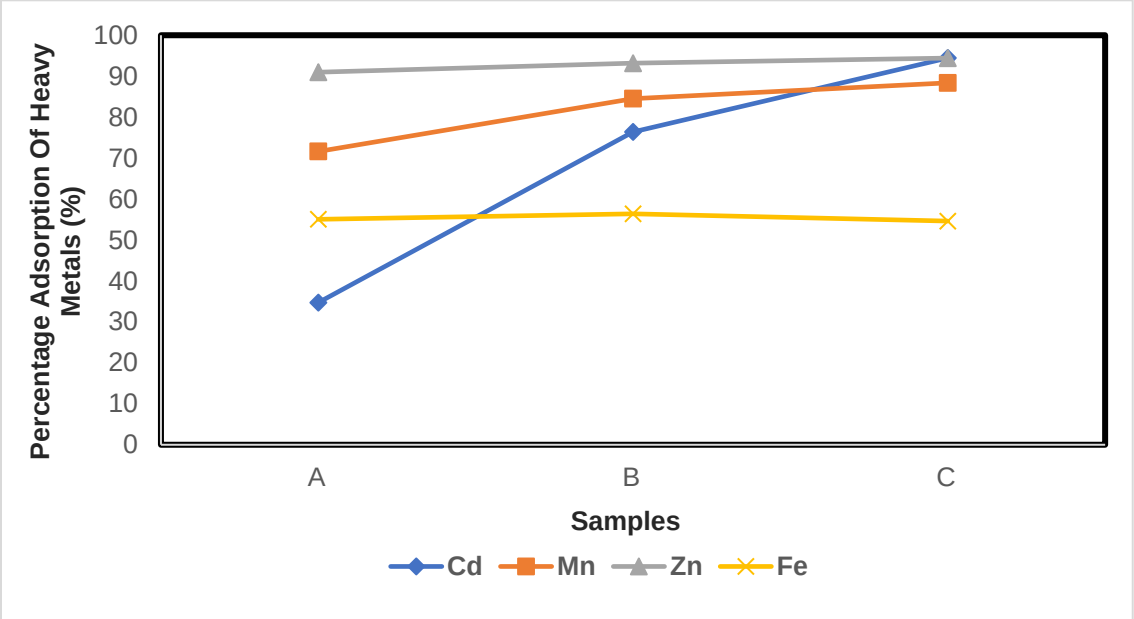

Fig. 12. Heavy metals removal effectiveness by three different compositions of developed composite PLA / TiO_2 / GB

COD, TSS, and turbidity properties

Figure 13 and Table 8 distinguished the removal percentages of COD, TSS, and turbidity in POME after applying samples A, B, and C. Certain studies have found that composite dosage significantly influences the adsorption ability of pollutants (Zha *et al*. 2018; Ng *et al*. 2019; Upender and Kishore 2021). The initial pH of the raw POME in this study was 4.4, with its COD, TSS, and turbidity recorded at 2584 mg/L, 545 mg/L, and 1876 NTU, respectively.

Table 8. Comparison between the Initial and Final Condition of POME

Parameters	POME Initial Condition	Standard discharge limit based on the Malaysian Department of Environment	POME Final Condition			Removal (%)		
			Sample A	Sample B	Sample C	Sample A	Sample B	Sample C
Chemical oxygen demand (mg/L)	2584	-	1648	1552	1567	36	40	39
Total suspended solids (mg/L)	545	400	540	452	376	1	17	31
Turbidity (NTU)	1876	-	946	837	723	40	55.38	61.5
pH	4.4	5-9	5.78	6.40	6.68	-	-	-

Similar to Ng *et al.* (2019), the presence of high levels of organic compounds and suspended solids in the POME resulted in increased turbidity and an unpleasant dark colour solution. The combination of TiO_2 and GB demonstrated a synergistic effect. The photocatalytic characteristic of TiO_2 in each sample aids in improving the colour of POME to light yellowish from dark brown caused by the degradation of organic contaminants such as lignin in the POME after 48 h of contact time. Utami *et al*. (2019) investigated the effect of TiO_2 dosage on COD, TSS, and turbidity levels. They discovered that a high dosage of TiO_2 nanoparticles with a large surface area could enhance the degradation process of organic pollutants due to the increased possibility of direct contact between TiO_2 and pollutants. Figure 13 shows that a significant reduction in TSS and turbidity concentrations were observed with increasing GB dosage, as demonstrated by samples A, B, and C. According to Zamawi *et al*. (2018), increasing the content of GB improves the total active site presence, allowing more Van der Waals interaction between pollutants and GB surfaces. As a result, more contaminants will be attracted to the surface of GB, increasing the diffusion rate between impurities and the TiO_2 surface. Additionally, the TiO_2 could initiate the oxidation of pollutants and increase total degradation (Maneerung *et al*. 2016). Based on the comparison of samples A, B, and C in Table 8, the application of sample A resulted in the lowest reduction percentages of COD, TSS, and POME turbidity, indicating that it was less efficient than samples B and C. Figure 13 displays the results of sample A, which remained at the highest levels of COD, TSS, and turbidity concentration. This could be due to the inadequate adsorption sites in GB of sample A, limiting the formation of bridges between adjacent particles and resulting in the re-stabilization of pollutants (Teh *et al*. 2016).

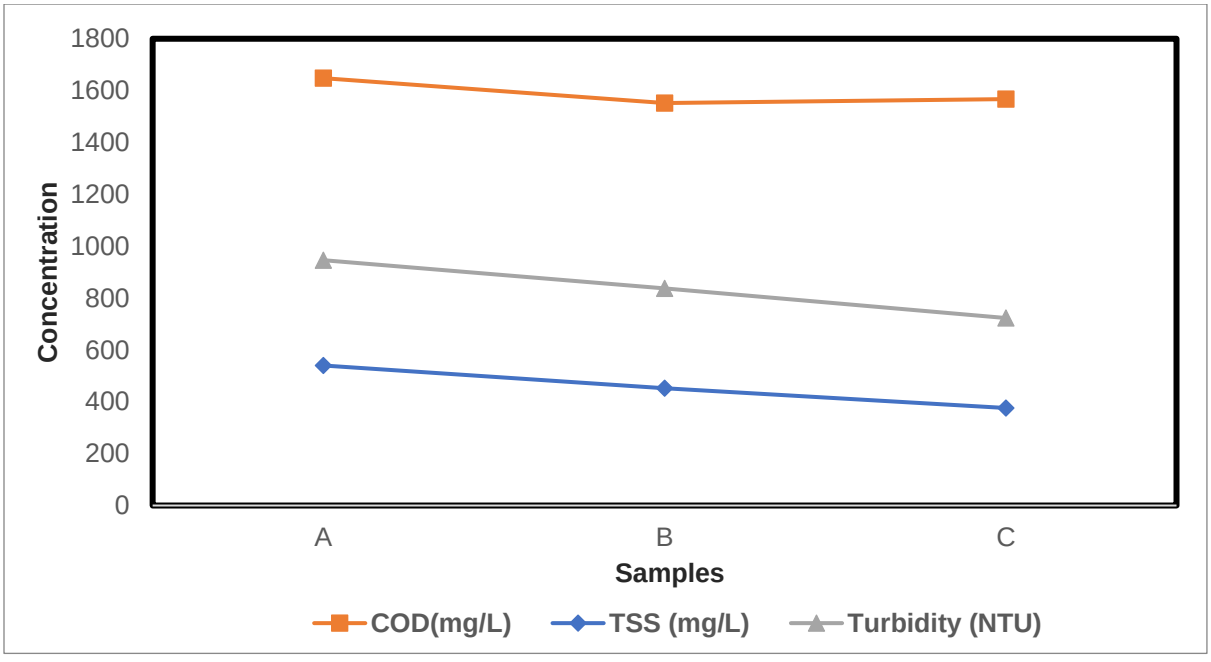

Fig. 13. Effect of the developed composites on COD, TSS, and turbidity of POME

Sample C accounted for the highest TSS reduction of 31% compared to samples A and B, although not much TSS removal was recorded. The content of GB also aided in lowering the turbidity, where the cloudiness of the POME has been improved compared to

their initial. As stated by Casalini *et al*. (2019), the negative charge of PLA particles has allowed it to neutralize the cations present in the POME, causing deposition of contaminants on the adsorbent and increasing the adsorption rate of organic molecules from POME. Another factor that influenced the degradation of organic compounds was the pH value of POME (Arutanti *et al*. 2020). Aruntanti *et al.* (2020) and Farraji *et al*. (2017) stated that lignin degradation in POME was observed with the formation of intermediate products. This result is reflected in the FTIR analysis presented in Fig. 3, where the benzene ring of lignin deformation was observed.

CONCLUSIONS

1. There were functional groups such as carbonyl (=C=O), hydroxyl (-OH), amide (N H_2), and phenolic (Ph-OH) in the ground biochar (GB) sample. These functional groups improve the adsorption properties.
2. The Fourier transform infrared (FTIR) results of composites prepared with poly(lactic acid), titanium dioxide, and GB (PLA / TiO_2 / GB) revealed the degradation of lignin in palm oil mill effluent (POME), which indirectly improves the quality of effluent.
3. The H_2SO_4 acid reagent has several advantages. The chemical activation increased the surface area of the ground biochar activated carbon. The development of the pores resulted in more active sites for adsorbate molecules.
4. Sample C demonstrated the highest adsorption efficiency with a reduction of 94.4% Mn, 88.4% Cd, and 94.4% Zn from untreated POME.
5. There was a higher removal of chemical oxygen demand (COD), total suspended solids (TSS), and turbidity of POME due to the high weightage of GB compared to samples B and C.
6. The results were correlated with the outcomes of the ball milling process and the use of PLA and TiO_2. In addition, the application of sample C in treating the POME improved the pH level of POME to nearly neutral, from 4.4 to 6.68.

ACKNOWLEDGEMENTS

The first author wishes to express her heartfelt appreciation to all individuals, parties, and organizations who contributed to this study, especially the Department of Chemical Engineering and Energy Sustainability, Faculty of Engineering, Universiti Malaysia Sarawak. This research work was funded by Institutional Fund Projects under grant no (IFPIP-477-130-1443). The authors gratefully acknowledge technical and financial support provided by the ministry of Education and King Abdulaziz University, DSR, Jeddah, Saudi Arabia

REFERENCES CITED

Abbar, B., Alem, A., Marcotte, S., and Duriatti, D. (2017). "Experimental investigation on removal of heavy metals (Cu^{2+}, Pb^{2+} and Zn^{2+}) from aqueous solution by flax fibres," *Process Safety and Environmental Protection* 109(1). 639-647. DOI: 10.1016/j.psep.2017.05.012

Abbas, A., Hu, K.C., Lin, H.C., and Lin, K.M. (2021). "Effects of ball milling and additives (activated carbon and copper) on hydrogen adsorption characteristics of ZK60 alloy," *Materials Chemistry and Physics* 271(1). 1-15. DOI: 10.1016/j.matchemphys.2021.124950

Abel, S., Loh, S., Wahab, N., Masek, O., Tanimu, M., and Bacmann, R. (2021). "Effect of operating temperature on physicochemical properties of empty fruit bunch cellulose-derived biochar," *Journal of Oil Palm Research* 33(4) 643-652. DOI: 10.21894/jopr.2021.0007

Adeleke, A. O., Al-Gheethi, A. A., and Daud, Z. (2017). "Optimization of operating parameters of novel composite adsorbent for organic pollutants removal from POME using response surface methodology," *Chemosphere* 174(1), 232-242. DOI: 10.1016/j.chemosphere.2017.01.110

Ahmad, A., and Azam, T. (2019). "Water purification technologies," in: *Bottled and Packaged Water*, A. M. Grumezescu and A. M. Holban (eds.), Woodhead Publishing, Sawston, UK. DOI: 10.1016/B978-0-12-815272-0.00004-0

Alam, S., Khan, M., Bibi, W., Zekker, I., Burlakovs, J., Ghangrekar, M., and Zahoor, M. (2021). "Preparation of activated carbon from the wood of Paulownia tomentosa as an efficient adsorbent for the removal of acid red 4 and methylene blue present in wastewater," *Water* 13(11), 1-15. DOI: 10.3390/w13111453

Alfattani, R., Shah, M., Siddiqui, M., Ali, M., and Alnaser, I. (2022). "Biochar characterization produced from walnut shell biomass through slow pyrolysis," *Energies* 15(1) 1-15. DOI: 10.3390/en15010001

Ali, S., and Latip, J. (2020). "Rapid investigation of the metabolite content in *Hibiscus sabdariffa* var. UKMR-2 cultivated under the influence of elevated CO_2 using tri-step FT-IR spectroscopy," *Jurnal Teknologi* 83(1), 75-83. DOI: 10.11113/jurnalteknologi.v83.14825

Allwar, A. (2012). "Characteristic of pore structures and surface chemistry of activated carbons by physisorption, FTIR and Boehm methods," *IOSR Journal of Applied Chemistry* 2(1), 9-15. DOI: 10.9790/5736-0210915

AlMoharbi, S., Devi, M., Sangeetha, B., and Jahan, S. (2019). "Studies on the removal of copper ions from industrial effluent by *Azadirachta indica* powder," *Applied Water Science* 10(1)-1-15. DOI: 10.1007/s13201-019-1100-z

Alsawy, T., Rashad, E., El-Qelish, M. and Mohammed, R. H. (2022). "A comprehensive review on the chemical regeneration of biochar adsorbent for sustainable wastewater treatment," (2022). *NPJ Clean Water* 5, 29. DOI: 10.1038/s41545-022-00172-3

Arutanti, O., Sari, A., Berkah, A., Nurdin, M., Fitriady, M., Parmawati, Y., and Hadibarata, T. (2020). "Advanced degradation of lignin from palm oil mill effluent (POME) by a combination of photocatalytic-Fenton treatment and TiO_2 nanoparticle as the catalyst," *Water Air and Soil Pollution* 231(1), 1-20. DOI: 10.1007/s11270-020-04617-8

ASTM D6556-14 (2014). "Standard test method for carbon black-Total and external surface area by nitrogen adsorption," ASTM International, West Conshohocken, PA, USA.

ASTM D7440-20 (2020). "Standard practice for optimization, calibration, and validation of atomic absorption spectrometry for metal analysis of petroleum products and lubricants," ASTM International, West Conshohocken, PA, USA.

ASTM E1252-98 (2021). "Standard practice for general techniques for obtaining infrared spectra for qualitative analysis," ASTM International, West Conshohocken, PA, USA.

ASTM E168-16 (2016). "Standard practices for general techniques of infrared quantitative analysis," ASTM International, West Conshohocken, PA, USA.

ASTM E2015-04 (2014). "Standard guide for preparation of plastics and polymeric specimens for microstructural examination," ASTM International, West Conshohocken, PA, USA.

Aziz, R., Li, C., Salleh, M., and Saleh, M. (2021). "Removal of iron and manganese from palm oil mill effluent (POME) using activated clinoptilolite zeolite," *IOP Conference Series: Earth and Environmental Science* 765(1), 1-20. DOI: 10.1088/1755-1315/765/1/012029

Baskar, A. V., Bolan, N., Hoang, S. A., Sooriyakumar, P., Kumar, M., Singh, L., Jasemizad, T., Padhye, L. P., Singh, G., Vinu, A., Sarkar, B., Kirkham, M.B., Rinklebe, J., Wang, S., Wang, H., Balasubramanian, R., and Siddique, K. H. M. (2022). "Recovery, regeneration and sustainable management of spent adsorbents from wastewater treatment streams: A review," *Science of the Total Environment* 822, article 153555. DOI: 10.1016/j.scitotenv.2022.153555

Bilal, M., Shah, J., Ashfaq, T., Gardazi, S., Tahir, A., Pervez, H., and Mahmood, Q. (2013). "Waste biomass adsorbents for copper removal from industrial wastewater-a review," *Journal of Hazardous Material* 263(2), 322-333. DOI: 10.1016/j.jhazmat.2013.07.071

Buttersack, C., Mollmer, J., Hofmann, J., and Glaser, R. (2016). "Determination of micropore volume and external surface of zeolites," *Microporous and Mesoporous Materials* 236, 63-70. DOI: 10.1016/j.micromeso.2016.08.018

Casalini, T., Rossi Filippo, Castrovinci, A., and Perale, G. (2019). "A perspective on polylactic acid-based polymers use for nanoparticles synthesis and applications," *Frontiers* 7(1), 1-10. DOI: 10.3389/fbioe.2019.00259

Datta, J., Kosiorek, P., and Wloch, M. (2016). "Effect of high loading of titanium dioxide particles on the morphology, mechanical and thermo-mechanical properties of the natural rubber-based composites," *Iranian Polymer Journal* 25(1). 1021-1035 DOI: 10.1007/s13726-016-0488-7

Farraji, H., Zamana, N. Q., Saat, S., and Dashti, A. (2017). "Phytoremediation of suspended solids and turbidity of palm oil mill effluent (POME) by *Ipomea aquatica*," *Engineering Heritage Journal* 1(1). 36-40. DOI: 10.26480/gwk.01.2017.36.40

Feng, S., Yuan, Z., Leitch, M., and Xu, C. (2014). "Hydrothermal liquefaction of barks into bio-crude-effects of species and ash content/composition," *Fuel* 116(1), 214-220. DOI: 10.1016/j.fuel.2013.07.096

Gul, A., Khaligh, N. G., and Julkapli, N. M. (2021). "Surface modification of carbon-based nanoadsorbents for the advanced wastewater treatment," *Journal of Molecular Structure* 1235, article 130148. DOI: 10.1016/j.molstruc.2021.130148

Gupta, A., Sharma, V., Sharma, K., and Kumar, V. (2021). "A review of adsorbents for heavy metal decontamination: Growing approach to wastewater treatment." *Materials* 14(16), 1-20. DOI: 10.3390/ma14164702

Hidayu, A. R., Mohamad, N. F., Matali, S., and Sharifah, A. S. A. K. (2013). "Characterization of activated carbon prepared from oil palm empty fruit bunch using BET and FT-IR techniques," *Procedia Engineering* 68, 379-384. DOI: 10.1016/J.PROENG.2013.12.195

Hirschmann, R. (2022). "Palm oil industry in Malaysia – Statistics and facts," Viewed on 24 July, 2022, https://www.statista.com/topics/5814/palm-oil-industry-in-malaysia/#topicHeader__wrapper

Hu, S., Zhang, D., Yang, Y., Ran, Y., Mao, J., Chu, W., and Cao, X. (2019). "Effects of the chemical structure, surface and micropore properties of activated and oxidized black carbon on the sorption and desorption of phenanthrene," *Environmental Science Technology* 53(13), 7683-7693. DOI: 10.1021/acs.est.9b01788

Jagaba, A., Kutty, S., Hayder, G., Baloo, L., Ghaleb, A., Lawal, L., Abubakar, S., Al-dhawi, B. N. S., Al-Mahbashi, N. M. Y., and Umaru , I. (2020). "Degradation of Cd, Cu, Fe, Mn, Pb and Zn by Moringa-oleifera, zeolite, ferric-chloride, chitosan and alum in an industrial effluent," *Ain Shas Engineering Journal* 12(1), 57-64. DOI: 10.1016/j.asej.2020.06.016

Jahromi, F., and Ghahreman, A. (2019). "Effect of surface modification with different acids on the functional groups of AF 5 catalyst and its catalytic effect on the atmospheric leaching of enargite," *Colloids and Interfaces* 3(2), 1-25. DOI: 10.3390/colloids3020045

Kaman, S., Tan, I., and Lim, L. (2017). "Palm oil mill effluent treatment using coconut shell-based activated carbon: adsorption equilibrium and isotherm," *MATEC Web of Conferences* 87(1) 1-6. DOI: 10.1051/matecconf/20178703009

Kamyab, H., Chelliapan, S., Din, M., and Rezania, S. (2018). "Palm oil mill effluent as an environmental pollutant," in: Palm Oil, Waisundara, V.Y. (ed). InTechOpen, London, United Kingdom. DOI: 10.5772/intechopen.75811

Kaseem, M., Hamad, K., and Rehman, Z. U. (2019). "Review of recent advances in polylactic acid/TiO_2 composites," *Materials* 12(22), 1-10. DOI: 10.3390/ma12223659

Khamis, M., and Jalil, M. (2021). "Potential of banana stem as bio-adsorbent for palm oil mill effluent (POME) treatment," *Progress in Engineering Application and Technology* 2(1), 62-73.

Kowalczuk, D., and Pitucha, M. (2019). "Application of FTIR method for the assessment of immobilization of active substances in the matrix of biomedical materials," *Materials* 12(18), 1-10. DOI: 10.3390/mal12182972

Kumar, R., Rauwel, P., and Rauwel, E. (2021). "Nanoadsorbents for the removal of heavy metals from contaminated water: Current scenario and future directions," *Processes* 9(8), article 1379. DOI: 10.3390/pr9081379

Lim, A., Chew, J., Ngu, L., Ismadji, S., Khaerudini, D., and Sunarso, J. (2020). "Synthesis, characterization, adsorption isotherm and kinetic study of oil palm trunk-derived activated carbon for tannin removal from aqueous solution," *ACS Omega* 5(44), 28673-28683. DOI: 10.1021/acsomega.0c03811

Lyu, H., Gao, B., He, F., Zimmerman, A., Ding, C., Huang, H., and Tang, J. (2018). "Effects of ball milling on the physicochemical and sorptive properties of biochar: Experimental observations and governing mechanisms." *Environmental Pollution* 233(1), 54-63. DOI: 10.1016/j.envpol. 2017.10.037

Mahesh, N., Balakumar, S., Shyamalagowri, S., Manjunathan, J., Pavithra, M. K. S., Babu, P. S., Kamaraj, M., and Govarthanan, M. (2022). "Carbon-based adsorbents as proficient tools for the removal of heavy metals from aqueous solution: A state of art-review emphasizing recent progress and prospects," *Environmental Research* 213, article 113723. DOI: 10.1016/j.envres.2022.113723

Matteis, V., Cannavale, A., and Ayr, U. (2020). "Titanium dioxide in chromogenic devices: Synthesis, toxicological issues and fabrication methods," *Applied Sciences* 10(24), 1-15. DOI: 10.3390/app10248896

Maneerung, T., Liew, J., Dai, Y., Kawi, S., Chong, C., and Wong, C. (2016). "Activated carbon derived from carbon residue from biomass gasification and its application for dye adsorption: kinetics, isotherms and thermodynamic studies," *Bioresource Technology* 200(1), 350-359. DOI: 10.1016/j.biortech.2015.10.047

Mohammad, S., Baidurah, S., Kobayashi, T., Ismail, N., and Leh, C. (2021). "Palm oil mill effluent treatment processes," *Processes*, 9(5), 1-22. DOI: 10.3390/pr9050739

Moosavi, S., Lai, C. W., Gan, S., Zamiri, S., Pivehzhani, O. A., and Johan, M. R. (2020). "Application of efficient magnetic particles and activated carbon for dye removal from wastewater," *ACS Omega* 5(33), 20684-20697. DOI: 10.1021/acsomega.0c01905

Mosunmola, A. G., and Olatunde, S. K. (2020). "Palm oil mill effluents (POME) and its pollution potentials: A biodegradable prevalence," *Journal of Pollution Effects and Control* 8(5), 258. DOI: 10.35248/2375-4397.20.8.258

Naayi, S., Hassan, A., and Salim, E. (2018). "FTIR and X-ray diffraction analysis of Al2O3 nanostructured thin film prepared at low temperature using spray pyrolysis method," *International Journal of Nanoelectronics and Materials* 11(12), 1-6.

Ng, W., Lai, S., Chong, K., Lee, S., Koo, C., and Chong, W. (2019). "Reduction of total suspended solids, turbidity and colour of palm oil mill effluent using hybrid coagulation-filtration process," *Journal of Applied Membrane Science and Technology* 23(1), 73-88. DOI: 10.11113/AMST.V23N1.144

Nyuk Khui, P. L., Rahman, M. R., Ahmed, A. S., King Kuok, K., Bakri, M. K.B., Tazeddinova, D., Kazhmukanbetkyzy, Z. A., and Baibatyrov Torebek, B. B. (2021). "Morphological and thermal properties of composites prepared with poly(lactic acid), poly(ethylene-alt-maleic anhydride), and biochar from microwave-pyrolyzed jatropha seeds," *BioResources* 16(2), 3171-3185. DOI: 10.15376/biores.16.2.3171-3185

Nyuk Khui, P. L., Rahman, M., Hamdan, S., Jayamani, E., Bakri, M. K. B., and Sanaullah, K. (2020). "Synthesis and characterization of micro-nano carbon filler from *Jatropha* seeds," *BioResources* 15(2), 3237-3251. DOI: 10.15376/biores.15.2.3237-3251

Pertile, E., Dvorsky, T., Vaclavik, V., and Heviankova, S. (2021). "Use of different types of biosorbents to remove Cr (VI) from aqueous solution," *Life* 11(3), 1-10. DOI: 10.3390/life11030240

Phanthong, P., Reubroycharoen, P., Hao, X., Xu, G., Abudula, A., and Guan, G. (2018). "Nanocellulose: Extraction and application," *Carbon Resources Conversion* 1(1), 32-43. DOI: 10.1016/j.crcon.2018.05.004

Phothong, K., Tangsathitkulchai, C., and Lawtae, P. (2021). "The analysis of pore development and formation of surface functional groups in bamboo-based activated carbon during CO_2 activation," *Molecules* 26(18) 1-10. DOI: 10.3390/molecules26185641

Qanytah, Q., Syamsu, K., Fahma, F., and Pari, G. (2020). "Characterization of ball-milled

bamboo-based activated carbon treated with KMnO4 and KOH as activating agents," *BioResources* 15(4), 8303-8322. DOI: 10.15376/biores.15.4.8303-8322

Raquez, J.-M., Habibi, Y., Murariu, M., Dubois, P. (2013). "Polylactide (PLA)-based Nanocomposites," *Progress in Polymer Science* 38(10-11), 1504-1542. DOI: 0.1016/j.progpolymsci.2013.05.014

Saffar, A., Carreau, P., Kamal, M. R., and Ajji, A. (2014). "Hydrophilic modification of polypropylene microporous membranes by grafting TiO_2 nanoparticles with acrylic acid groups on the surface," *Polymer* 55(23), 6069-6075. DOI: 10.1016/j.polymer.2014.09.069

Salema, A., Afzal , M., and Bennamoun, L. (2017). "Pyrolysis of corn stalk biomass briquettes in a scaled-up microwave technology," *Bioresource Technology* 233, 353-362. DOI: 10.1016/j.biortech.2017.02.113

Salim, R. M., Asik, J., and Sarjadi, M. (2021). "Chemical functional groups of extractives, cellulose and lignin extracted from native *Leucaena leucocephala* bark," *Wood Science and Technology* 55(1), 295-313. DOI: 10.1007/s00226-020-01258-2

Santos, D. H. S., Xiao, Y., Chaukura, N., Hill, J. M., Selvasembian, R., Zanta, C. L. P. S., and Meili, L. (2022). "Regeneration of dye-saturated activated carbon through advanced oxidative processes: A review," *Heliyon* 8(8), article e10205. DOI: 10.1016/j.heliyon.2022.e10205

Sayuti, N., Ali, R., and Anuar, T. (2021). "Synthesis and characterization of biobased epoxidized edible oils," *Universiti Malaysia Terengganu Journal of Undergraduate Research* 3(4) 195-206. DOI: 10.46754/umtjur.2021.10.020

Senturk, I., and Yildiz, M. (2020). "Highly efficient removal from aqueous solution by adsorption of Maxilon Red GRL dye using activated pine sawdust," *Korean Journal of Chemical Engineering* 37(1), 985-999. DOI: 10.1007/s11814-020-0526-1

Shaharuddin, S. I., Mukhtar, A., Akhir, N., Shaffiar, N., and Othman, M. (2019). "Experimental and finite element analysis of solvent cast poly(lactic acid) thin film blends," *IIUM Engineering Journal* 20(2), 197-210. DOI: 10.31436/iiumej.v20i2.1119

Shahbandeh, M. (2022). "Palm oil: global production," Volume 2012/13-2021/22. Viewed on 24 July, 2022, https://www.statista.com/statistics/613471/palm-oil-production-volume-worldwide/#:~:text=The%20global%20production%20of%20palm,exporters%20of%20palm%20oil%20worldwide.&text=Palm%20oil%20grows%20mainly%20in%20Asia%2C%20Africa%20and%20Latin%20America

Shan, D., Deng, S., Zhao, T., Wang, B., Huang, J., Yu, G., and Wiesner, M. (2016). "Preparation of ultrafine magnetic biochar and activated carbon for pharmaceutical adsorption and subsequent degradation by ball milling," *Journal of Hazardous Material* 305(1), 156-163. DOI: 10.1016/j.jhazmat.2015.11.047

Sreedhar, I., and Reddy, N. (2019). "Heavy metal removal from industrial effluent using bio-sorbent blends," *SN Applied Science* 1(1), 1-15. DOI:10.1007/s42452-019-1057-4

Taha, A., Shreadah, M., Ahmed, A., and Heiba, H. (2016). "Multi-component adsorption of Pb(II), Cd(II)), and Ni(II) onto Egyptian Na-activated bentonite; equilibrium, kinetics, thermodynamics and application for seawater desalination," *Journal of Environmental Chemical Engineering* 4(1), 1166-1180 DOI: 10.1016/j.jece.2016.01.025

Teh, C., Budiman, P., Shak, K., and Wu, T. (2016). "Recent advancement of coagulation-flocculation and its application in wastewater treatment," *Industrial and Engineering*

Chemistry Research 55(16), 4363-4389. DOI: 10.1021/acs.iecr.5b04703

Tran, H. N., Lee, C. K., Nguyen, T. V., and Chao, H. P. (2017). "Saccharide-derived microporous spherical biochar prepared from hydrothermal carbonization and different pyrolysis temperatures: Synthesis, characterization, and application in water treatment," *Environmental Technology* 39(21). DOI: 10.1080/09593330.2017.1365941

Upender, H., and Kishore, K. (2021). "A study on removal of dye, COD, turbidity and DO enhancement from synthetic textile wastewater by using natural adsorbent in RSM design; isothermal analysis," *Chemical Papers* 75(1), 5403-5420. DOI: 10.1007/s11696-021-01709-5

Utami, F., Rahman, D., Sutisna, Kamirul, Margareta, D., and Abdullah , M. (2019). "Photocatalyst based on TiO_2 and its application in organic wastewater treatment using simple spray method," *Journal of Physics* 1204(1), 1-15. DOI: 10.1088/1742-6596/1204/1/012086

Wijaya, M., and Wilharto, M. (2020). "Synthesis and characterization of bioactive compound from cocoa fruit shell by pyrolysis process," *Journal of Physics* 1567(1), 1-10. DOI: 10.1088/1742-6596/1567/2/022025

Xing, B., Shi, C., Zhang, C., Yi, G., Chen, L., Guo, H., and Cao, J. (2016). "Preparation of TiO2/activated carbon composites for photocatalytic degradation of RhB under UV light irradiation," *Journal of Nanomaterial* 2016(1), 1-10. DOI: 10.1155/2016/8393648

Zahari, M., Baharum, A., Anuar, F., and Othman, R. (2017). "Palm oil industry in South East Asia and the effluent treatment technology," *Environmental Technology and Innovation* 9(1), 169-185. DOI: 10.1016/j.eti.2017.11.003

Zain, N. M., Lim, C., Usman, A., Keasberry, N., Thotagamuge, R., and Mahadi, A. (2021). "Synergistic effect of TiO_2 size on activated carbon composites for ruthenium N-3 dye adsorption and photocatalytic degradation in wastewater treatment," *Environmental Nanotechnology, Monitoring and Management* 16(1). 1-10. DOI: 10.1016/j.enmm.2021.100567

Zamawi, A., Ramli, R., and Harun, N. (2018). "Synergistic effect of adsorption-photodegradation of composite TiO_2/AC for degradation of 1-butyl-3-methyl-imidazolium chloride," *Malaysian Journal of Analytical Sciences* 22(4), 648-658. DOI: 10.17576/mjas-2018-2204-11

Zha, Y., Wang, Y., Liu, S., Liu, S., Yang, Y., Jiang, H., and Wang, H. (2018). "Adsorption characteristics of organics in the effluent of ultra-short SRT wastewater treatment by single-walled, multi-walled and graphitized multi-walled carbon nanotubes," *Scientific Report* 8(1), 1-15. DOI: 10.1038/s41598-018-35374-8

Article submitted: February 1, 2023; Peer review completed: May 20, 2023; Revised version received: June 12, 2023; Accepted: June 20, 2023; Published: July 3, 2023.
DOI: 10.15376/biores.18.3.5548-5573